Supporting Information

of the **Advanced Functional Materials** paper:

Single Component Self-Assembled Monolayers of Aromatic Azo-biphenyl: Influence of the Packing Tightness on the SAM Structure and Light Induced Molecular Movements

By Mark Elbing, Alfred Błaszczyk, Carsten von Hänisch, Marcel Mayor, Violetta Ferri, Christian Grave, Maria Anita Rampi, Giuseppina Pace, Paolo Samorì, Andrei Shaporenko, Michael Zharnikov

Content:

1. Synthesis and Characterization of AZO1 and AZO2 and Intermediates

General: All chemicals were used as received from the supplier, solvents were p.a. quality and used without further purification. Dry 3-dimethyl-2-imidazolidinone (DMI) was purchased from Fluka. If necessary the solvents were dried by standard literature procedures, THF, diethylether and toluene with Na/benzophenone, CH_2Cl_2 and all amines over CaH_2, ethanol using magnesium turnings. If not mentioned otherwise all reactions were carried out under an atmosphere of nitrogen or argon. ^{1}H-NMR and ^{13}C-NMR spectra were recorded on a Bruker Ultra Shield 300 MHz, the J values are given in Hz. If temperatures other than room temperature were used, the reading of the thermocouple of the instrument is quoted. MALDI-TOF MS spectra were recorded on a time-of-flight mass spectrometer (PerSeptive Biosystems Voyager -DE PRO). EI-MS were recorded on a Finnigan MAT 95Q mass spectrometer. Melting points were measured with a Büchi Melting Point B-540 apparatus. TLC was performed on Merck silica gel 60 F_{254} plates and column chromatography using Merck silica gel 60 (0.040–0.063 mm). Elemental analyses were recorded using a ThermoQuest FlashEA 1112 N/Protein Analyzer.

4,4'-Diiodo-2,2'-dimethyl-biphenyl (**9**) was synthesized according to a literature procedure.[1]

4-Nitroso-biphenyl (**2**): 4-Nitro-biphenyl (**1**) (15.936 g, 80.00 mmol) was dissolved in methoxyethanol (400 ml) and a solution of NH_4Cl (6.793 g, 127.00 mmol) in H_2O (100 ml) was added. The reaction mixture was warmed to 30°C and finely powdered zinc (20.384 g, 311.72 mmol) was added in portions over a period of 30 min maintaining the temperature between 30-35°C while stirring vigorously using mechanical stirring. The mixture was allowed to react at 35°C for 2 h and then filtered and washed with methoxyethanol. The filtrate was added to a solution of $FeCl_3$ (25.200 g, 155.37 mmol) in H_2O (300 ml) and ethanol (120 ml) over the course of 90 min while the temperature was kept at -5°C. After 1 h the mixture was poured into water

(ca. 800 ml) and the yellow precipitate collected. It was dried and then dissolved in CH_2Cl_2 and filtered over silica gel. After evaporation of the solvents a dark orange solid was obtained that was purified by recrystallization from ethanol affording **2** as orange solid (9.266 g, 50.58 mmol; 63%). M.p.: 73.0-74.0 °C (Lit.:[2] 74 °C). ^{1}H-NMR (300 MHz, $CDCl_3$): δ = 7.45-7.54 (m, 3 H), 7.68 (td, ^3J(H,H) = 8 Hz, ^4J(H,H) = 2 Hz, 2 H), 7.83 (dd, ^3J(H,H) = 9 Hz, ^4J(H,H) = 1 Hz, 2 H), 7.98 (d, ^3J(H,H) = 9 Hz, 2 H). ^{13}C-NMR (75 MHz, $CDCl_3$): δ = 121.70 (C3), 127.51 (C2'), 127.89 (C3'), 128.67 (C4'), 129.16 (C2), 148.13 (C1), 165.00 (C4).

4'-Bromo-4-methylsulfanyl-biphenyl (**4**): Sodium methanethiolate (4.110 g, 0.059 mol) was dissolved in dry DMI (310 ml) and 4,4'-dibromo-biphenyl (**3**) (13.104 g, 0.042 mol) was added at once. The mixture was heated to 150 °C for 41 h. It was allowed to cool to room temperature and poured into sat. NaCl-solution (ca. 1200 ml). The aqueous phase was extracted with diethylether, and the combined ethereal layers were washed with water and dried over Na_2SO_4. Evaporation of the solvents under reduced pressure followed by column chromatography (CC) (silica gel, starting with hexane/toluene 15/1 increasing to hexane/toluene 4/1) yielded **4** as white solid (7.038 g, 0.025 mol; 60%). M.p.: 148.0-149.5°C (Lit.:[3] 148.0-150.0). ^{1}H-NMR (300 MHz, $CDCl_3$): δ = 2.52 (s, 3 H), 7.32 (td, ^3J(H,H) = 9 Hz, ^4J(H,H) = 2 Hz, 2 H), 7.43 (td, ^3J(H,H) = 9 Hz, ^4J(H,H) = 2 Hz, 2 H), 7.48 (td, ^3J(H,H) = 9 Hz, ^4J(H,H) = 2 Hz, 2 H), 7.55 (td, ^3J(H,H) = 9 Hz, ^4J(H,H) = 2 Hz, 2 H). ^{13}C-NMR (75 MHz, $CDCl_3$): δ = 16.19 (CH_3S), 121.80 (C4'), 127.30 (C3), 127.65 (C2), 128.80 (C2'), 132.31 (C3'), 137.11 (C1), 138.62 (C4), 139.85 (C1'). MS (EI): m/z (%) = 279.9, 277.9 (100) [M^+], 264.9, 262.9 (30) [M^+-CH_3], 184.0 (15) [M^+-Br, -CH_3], 152.1 [M^+-Br, -SCH_3]. Elemental analysis calcd. (%) for $C_{13}H_{11}BrS$ (279.20): C 55.92, H 3.97; found C 55.96, H 3.92.

4'-Bromo-4-methanesulfinyl-biphenyl (**5**): A solution of 4'-bromo-4-methylsulfanyl-biphenyl (**4**) (5.026 g, 18.00 mmol) in dry CH_2Cl_2 was cooled to 0°C using an ice/water bath. To the

cooled solution 3-chloroperoxybenzoic acid (*m*CPBA) (4.038 g, 23.40 mmol) was added in three portions and the mixture stirred at 0°C for 1 h. Then $Ca(OH)_2$ (2.222 g, 30.00 mmol) was added and the reaction mixture was stirred for additional 30 min at room temperature. The reaction mixture was filtered, washed with CH_2Cl_2 and the solvents removed *in vacuo*. The crude product was purified by CC (silica gel, ethyl acetate/toluene 9/1) giving **5** as white solid (4.732 g, 16.03 mmol; 89%). M.p.: 144.0-145.0°C. ^{1}H-NMR (300 MHz, $CDCl_3$): δ = 2.77 (s, 3 H), 7.47 (td, ^3J(H,H) = 9 Hz, ^4J(H,H) = 2 Hz, 2 H), 7.60 (td, ^3J(H,H) = 9 Hz, ^4J(H,H) = 2 Hz, 2 H), 7.71 (s, 4 H). ^{13}C–NMR (75 MHz, $CDCl_3$): δ = 44.02 (CH_3SO), 122.58 (C4'), 124.22 (C3), 127.92 (C2), 128.86 (C2'), 132.17 (C3'), 138.70 (C1'), 142.94 (C1), 144.89 (C4). MS (EI): *m/z* (%) = 295.9, 293.9 (55) [M^+], 280.8, 278.8 (100) [M^+-CH_3], 246.9 (21) [M^+-SCH_3], 152 (21) [M^+-Br, -$SOCH_3$]. Elemental analysis calcd. (%) for $C_{13}H_{11}BrOS$ (295.20): C 52.89, H 3.76; found: C 52.79, H 3.73.

4'-Methanesulfinyl-4-amino-biphenyl (**7**): A flame dried two necked flask was successively charged with $[Pd_2(dba)_3]\cdot CHCl_3$ (0.083 g, 0.08 mmol), BINAP (0.149 g, 0.24 mmol), compound **5** (2.362 g, 8.00 mmol), benzophenone imine (1.740 g, 9.60 mmol), NaO*t*Bu (1.076 g, 11.20 mmol) and dry toluene. The reaction mixture was heated to 80°C for 12 h. After cooling down to room temperature the reaction mixture was poured into Et_2O and filtered through a silica short plug with EtOAc as eluent. Evaporation of the solvents under reduced pressure and recrystallization from methanol afforded the crude diphenyl ketimine **6** as yellow solid (2.444 g, 6.18 mmol; 77%). The ketimine **6** was suspended in methanol and sodium acetate and hydroxylamine hydrochloride were added. After stirring the reaction for 2 h at r. t., it was poured into 0.1 M NaOH-solution. The aqueous phase was extracted with CH_2Cl_2 and the collected organic phases were dried over Na_2SO_4. The crude product was obtained by evaporation of the solvents and purification by CC (silica gel, EtOAc/toluene 9/1) afforded **7** as yellowish solid

(0.657 g, 2.84 mmol; 95%). M.p.: 191.0-192.0°C. ^{1}H-NMR (300 MHz, $CDCl_3$): δ = 2.75 (s, 3 H), 3.82 (br, 2 H), 6.82 (td, ^{3}J(H,H) = 9 Hz, ^{4}J(H,H) = 2 Hz, 2 H), 7.43 (td, ^{3}J(H,H) = 9 Hz, ^{4}J(H,H) = 2 Hz, 2 H), 7.67 (s, 4 H). ^{13}C-NMR (75 MHz, $CDCl_3$): δ = 44.03 (CH_3SO), 115.41 (C3), 124.03 (C3'), 127.14, 128.21 (C2', C2), 129.83 (C1), 143.05 (C1'), 144.18 (C4'), 146.71 (C4). MS (EI): *m/z* (%) = 231 (60) [M^+], 216 (100) [M^+-CH_3], 184.0 (10) [M^+-SCH_3]. Elemental analysis calcd. (%) for $C_{13}H_{13}NOS$ (231.31): C 67.50, H 5.66, N 6.06; found: C 67.58, H 5.88, N 5.92.

Biphenyl-4-yl-(4'-methanesulfinyl-biphenyl-4-yl)-diazene (**8**): 4-Nitroso-biphenyl (**2**) (0.572 g, 3.12 mmol) and compound **7** (0.657 g, 2.84 mmol) were dissolved in CH_2Cl_2 (25 ml) and AcOH (75 ml) and the reaction mixture was heated to 65°C for 67 h. The solvents were removed by rotary evaporation leaving a dark orange solid which was recrystallized from toluene affording **8** as red–brown solid (0.935 g, 2.36 mmol; 83%). M.p.: 270.0–272.0°C. ^{1}H-NMR (300 MHz, $CDCl_3$, T = 48°C): δ = 2.78 (s, 3 H), 7.39 (t, ^{3}J(H,H) = 8 Hz, 1 H), 7.48 (t, ^{3}J(H,H) = 8 Hz, 2 H), 7.68 (d, ^{3}J(H,H) = 8 Hz, 2 H), 7.75 – 7.79 (m, 6 H), 7.83 (d, ^{3}J(H,H) = 8 Hz, 2 H), 8.02-8.06 (m, 4 H). ^{13}C-NMR (75 MHz, $CDCl_3$, T = 48°C): δ = 44.03 (CH_3SO), 123.45, 123.52, 124.16, 127.18, 127.79, 127.91, 127.94, 128.09, 128.88, 140.25, 142.13, 143.22, 144.03, 145.55, 151.98, 152.55 (Ar). MALDI-ToF-MS: 396.77 [M^+]. Elemental analysis calcd. (%) for $C_{25}H_{20}N_2OS$ (396.51): C 75.73, H 5.08, N 7.07; found: C 75.57, H 5.26, N 6.80.

4'-(Biphenyl-4-ylazo)-biphenyl-4-thiol (**AZO1**): Compound **8** (0.119 g, 0.30 mmol) was dissolved in dry, argon saturated (Ar.-satd.) toluene (170 ml) and the mixture was heated to 40°C. Trifluoroacetic anhydride (0.752 g, 0.5 ml, 3.5 mmol) was added dropwise and the reaction was kept at 40°C for 2.5 h. The volatile solvents were removed by rotary evaporation and the residue was co-evaporated with dry toluene (2x 20 ml) to remove residual trifluoroacetic acid and anhydride. The obtained dark red solid was dried at HV for 1 h. Dry Ar.-satd. toluene (200 ml) and dry, Ar.-satd. EtOH (60 ml) was added followed by triethylamine (3.5 ml). The mixture was

stirred at r. t. for 88 h. The solvents were removed *in vacuo*, the residue dissolved in CH_2Cl_2, and washed twice with Ar.-satd. sat. NH_4Cl-solution, once with Ar.-satd. H_2O, dried over Na_2SO_4 and then filtered over a small column (silica gel, CH_2Cl_2). After rotary evaporation an orange solid was obtained which was recrystallized from toluene/EtOH 3/1 to afford **AZO1** as orange solid (0.030 g, 0.08 mmol; 27%). M.p.: 290.0°C (decomp.). ^{1}H-NMR (300 MHz, $CDCl_3$, T = 48°C): δ = 3.53 (s, 1 H), 7.37 – 7.39 (m, 3 H), 7.48 (t, ^3J(H,H) = 7 Hz, 2 H), 7.56 (t, ^3J(H,H) = 8 Hz, 2 H), 7.67-7.78 (m, 6 H), 8.00-8.04 (m, 4 H). MALDI–TOF–MS: 366.75 [M^+]. Elemental analysis calcd. (%) for $C_{24}H_{18}N_2S$ (366.48): C 78.66, H 4.95, N 7.64; found: C 78.36, H 5.18, N 7.26.

4'-*tert*-Butylsulfanyl-4-iodo-2,2'-dimethylbiphenyl (**10**): 4,4'-Diiodo-2,2'-dimethylbiphenyl (**9**) (4.084 g, 8.83 mmol) and sodium 2-methyl-2-propanethiolate (1.0897 g, 9.72 mmol) were dissolved in dry DMI (40 mL). The mixture was heated to 110°C for 13h. Then it was allowed to cool to room temperature, poured into sat. NaCl solution, the aqueous phase extracted with toluene. The organic layers were washed with water and then the solvent removed by rotary evaporation. The residue was purified by CC (silica gel, hexane/toluene 15/1) affording **10** as colorless oil (1.65 g, 4.15 mmol; 47%). ^{1}H NMR (300 MHz, $CDCl_3$): δ = 1.33 (s, 9 H), 2.00 (s, 3 H), 2.04 (s, 3 H), 6.84 (d, ^3J(H,H) = 8.0 Hz, 1 H), 7.02 (d, ^3J(H,H) = 7.6 Hz, 1 H), 7.38 (dd, ^3J(H,H) = 7.8 Hz, ^4J(H,H) = 1.4 Hz, 1 H), 7.44 (s, 1 H), 7.56 (dd, ^3J(H,H) = 8.0 Hz, ^4J(H,H) = 1.3 Hz, 1 H), 7.64 (s, 1 H); ^{13}C NMR (75 MHz, $CDCl_3$): δ = 19.59, 19.87, 31.19, 46.00, 93.08, 129.30, 131.06, 131.74, 134.76, 134.83, 136.05, 138.43, 138.80, 138.94, 140.67, 141.02; elemental analysis calcd (%) for $C_{18}H_{21}S$ (396.33): C 54.55, H 5.34; found: C 54.49, H 5.28; MS (EI): m/z (%) 395.9 (18) [M^+], 339.9 (100) [M^+-C_4H_8].

4'-*tert*-Butylsulfanyl-2,2'-dimethylbiphenyl-4-ylamine (**12**)**:** A pre-dried two necked flask was successively charged with $[Pd_2(dba)_3]\bullet CHCl_3$ (0.0405 g, 0.039 mmol), BINAP (0.073 g, 1.17 mmol), compound **10** (1.55 g, 3.91 mmol), benzophenone imine (0.8 ml, 4.7 mmol), NaO*t*Bu

(0.658 g, 5.86 mmol) and dry, degassed toluene (20 mL). Then the mixture was heated to 80°C for 4h. After that the solvent was removed, and the red, sticky oil was purified by filtration through a short column (silica gel, hexane/ether 4/1) giving **11** as yellow oil (1.72 g, 3.83 mmol; 98%), This was dissolved in methanol (50 mL) and sodium acetate (0.784 g, 9.55 mmol) and hydroxylamine hydrochloride (0.531 g, 7.64 mmol) were added and the reaction was stirred at room temperature for 2h. It was poured into 0.1M NaOH-solution and extracted with CH_2Cl_2. The collected organic phases were dried over Na_2SO_4 and evaporated to dryness. The yellow residue was purified by CC (silica gel, hexane/ether 1/1) to afford **12** as yellowish oil (0.825 g, 2.89 mmol; 74%). ^{1}H NMR (300 MHz, $CDCl_3$): δ = 1.33 (s, 9 H), 1.97 (s, 3 H), 2.07 (s, 3 H), 3.63 (br, 2 H), 6.57 (dd, ^3J(H,H) = 8.0 Hz, ^4J(H,H) = 2.4 Hz, 1 H), 6.59-6.63 (m, 1 H), 6.88 (d, ^3J(H,H) = 8.0 Hz, 1 H), 7.05 (d, ^3J(H,H) = 7.7 Hz, 1 H), 7.35 (dd, ^3J(H,H) = 8.0 Hz, ^4J(H,H) = 1.8 Hz, 1 H), 7.42 (s, 1 H); ^{13}C NMR (75 MHz, $CDCl_3$): δ = 19.95, 19.98, 31.27, 45.81, 112.67, 116.66, 130.26, 131.01, 131.73, 134.54, 136.86, 136.90, 138.73, 142.44, 145.64; elemental analysis calcd (%) for $C_{18}H_{23}NS$ (285.45): C 79.96, H 6.71, N 6.22; found: C 79.64, H 6.40, N 6.07; MS (EI): m/z (%) 285.1 (34) [M^+], 229.1 (100) [M^+-C_4H_8].

Biphenyl-4-yl-(4'-*tert*-butylsulfanyl-2,2'-dimethylbiphenyl-4-yl)-diazene (13): A solution of compound **12** (0.80 g, 2.80 mmol) and 4-nitrosobiphenyl (**2**) (0.6156 g, 3.36 mmol) in a mixture of glacial acetic acid/dichloromethane (75 ml/25 mL) was heated at 65°C for 16h. Then all solvents were removed and the brown residue was filtered through silica gel with hexane/ether (1/1). It was recrystallized from ethanol to give **13** as orange crystals (1.047 g, 2.324 mmol; 83%). M.p.: 157.5-158.5°C; ^{1}H NMR (300 MHz, $CDCl_3$): δ = 1.36 (s, 9 H), 2.11 (s, 3 H), 2.17 (s, 3 H), 7.11 (d, ^3J(H,H) = 7.7 Hz, 1 H), 7.28 (d, ^3J(H,H) = 8.0 Hz, 1 H), 7.36-7.55 (m, 5 H), 7.69 (d, ^3J(H,H) = 7.3 Hz, 2 H), 7.77 (d, ^3J(H,H) = 8.5 Hz, 2 H), 7.83 (dd, ^3J(H,H) = 8.1 Hz, ^4J(H,H) = 1.6 Hz, 1 H), 7.87 (s, 1 H), 8.03 (d, ^3J(H,H) = 8.5 Hz, 2 H); ^{13}C NMR (75 MHz, $CDCl_3$): δ =

20.18, 20.36, 46.31, 120.76, 123.78, 124.53, 127.62, 128.23, 128.32, 129.34, 129.53, 130.47, 132.02, 135.04, 136.38, 137.38, 139.25, 140.62, 141.77, 144.05, 144.38, 152.28, 152.50; elemental analysis calcd (%) for $C_{30}H_{30}N_2S$ (450.64): C 79.96, H 6.71, N 6.22; found: C 79.64, H 6.40, N 6.07; MS (MALDI-TOF): found: m/z 450.6692, calculated for $C_{30}H_{30}N_2S$ 450.2124.

1,2-bis(4'-(biphenyl-4-yldiazenyl)-2,2'-dimethylbiphenyl-4-yl)disulfane AZO2 And Thio-acetic acid S-[4'-(biphenyl-4-ylazo)-2,2'-dimethylbiphenyl-4-yl] ester AZO2': To a well-stirred solution of compound **13** (0.64 g, 1.44 mmol) in acetyl chloride/acetic acid (80 ml/0.5 ml), a solution of bromine (24.5 ml) in acetyl chloride/acetic acid (1/1) was added in 30 minutes at room temperature. The progress of the reaction was monitored by thin layer chromatography. After completion of the reaction (30 minutes after the bromine addition), all solvents were removed by evaporation and the crude residue was purified by CC (silica gel, hexane/CH_2Cl_2 1/1). Two fractions were collected; the first fraction was an orange solid identified as the disulfide **AZO2** (0.402 g, 1.022 mmol; 71%) and the second one was an orange solid identified as the acetyl substituted derivative **AZO2'** (0.119 g, 0.274 mmol; 19%). **AZO2:** M.p.: 223-224°C; ^{1}H NMR (300 MHz, $CDCl_3$): δ = 2.12 (s, 6 H), 2.19 (s, 6 H), 7.14 (d, ^3J(H,H) = 7.6 Hz, 2 H), 7.26 (d, ^3J(H,H) = 8.0 Hz, 2 H), 7.38-7.54 (m, 10 H), 7.69 (d, ^3J(H,H) = 8.3 Hz,4 H), 7.78 (d, ^3J(H,H) = 8.3 Hz, 4 H), 7.83 (d, ^3J(H,H) = 8.5 Hz, 2 H), 7.87 (s, 2 H), 8.03 (d, ^3J(H,H) = 8.1 Hz, 4 H); ^{13}C NMR (75 MHz, $CDCl_3$): δ = 20.08, 20.14, 120.52, 123.50, 124.25, 125.02, 127.33, 127.94, 128.05, 129.05, 129.09, 130.01, 130.32, 136.27, 136.99, 137.21, 140.19, 140.32, 143.82, 143.84, 151.97, 152.22; elemental analysis calcd (%) for $C_{52}H_{42}N_4S_2$ (787.05): C 79.35, H 5.38, N 7.12; found: 79.38, H 5.68, N 6.85; MS (MALDI-TOF): found: m/z 786.7094, calculated for $C_{52}H_{42}N_4S_2$ 786.2845. **AZO2'**: M.p.: 137.5-139.5°C; ^{1}H NMR (300 MHz, $CDCl_3$): δ = 2.11 (s, 3 H), 2.18 (s, 3 H), 2.46 (s, 3 H), 7.20 (d, ^3J(H,H) = 7.8 Hz, 1 H), 7.28 (d overlapped by solvent, 1 H), 7.32 (d, ^3J(H,H) = 8.4 Hz, 1 H), 7.36 (s, 1 H), 7.41 (d, ^3J(H,H) = 7.5 Hz, 1 H), 7.49 (t,

^{3}J(H,H) = 7.7 Hz, 2 H), 7.68 (d, ^{3}J(H,H) = 8.1 Hz, 2 H), 7.77 (d, ^{3}J(H,H) = 7.8 Hz, 2 H), 7.82 (s, ^{3}J(H,H) = 8.4 Hz, 1 H), 7.86 (s, 1 H), 8.02 (d, ^{3}J(H,H) = 8.4 Hz, 2 H); ^{13}C NMR (75 MHz, $CDCl_3$): δ = 19.93, 20.10, 30.38, 120.53, 123.50, 124.27, 126.93, 127.33, 127.93, 128.03, 129.04, 130.06, 130.16, 131.78, 135.89, 137.07, 137.12, 140.33, 142.26, 143.67, 143.85, 151.99, 152.29, 194.40; elemental analysis calcd (%) for $C_{28}H_{24}N_2OS$ (436.57): C 77.03, H 5.54, N 6.42; found: 76.81, H 5.50, N 6.22; MS (MALDI-TOF): found: m/z 436.7111, calculated for $C_{28}H_{24}N_2OS$ 436.1604.

2. Photochemical Characterization

a) UV-Vis Spectroscopy and Photo-Irradiation

UV-Vis spectra of both **AZO1** and **AZO2** in chloroform solutions were recorded with a Kontron Uvikon 931spectrophotometer. UV-Vis spectra of the solution samples from 1.64 to 1.09 x 10^{-4} M were recorded in a standard a quartz cell (10mm path) without degassing.

The photoisomerization studies of **AZO1** and **AZO2** in solution has been followed by recording the spectral variations under irradiation *in situ*. Chloroform solutions of **AZO1** and **AZO2** were irradiated by using a Spectraluminator LOT Oriel (power lamp 8.79 mW/cm^2) at λ = 370 and λ = 360 nm, respectively. The irradiation times are indicated in the main body of the text. The scan speed was 500 nm/min. The bandwidth of the light source in the UV-Vis region was 5 nm.

For UV-Vis measurements, Pt and Au films with a nominal thickness of 10 nm have been prepared on quartz by E-Beam deposition and vacuum sublimation, respectively. The SAMs were prepared by immersion of freshly prepared metallic substrates into a 0.1 mM solution of **AZO1** or **AZO2** in degassed chloroform at room temperature for 24–48 h. After immersion, the samples were carefully rinsed with pure chloroform and blown dry with argon.

UV-Vis spectra have been recorded with a Kontron Uvikon 931 spectrophotometer. The irradiation of the SAMs of **AZO1** and **AZO2** has been performed *in situ* inside the spectrophotometer cavity. The irradiation cycles have been executed with a Spectraluminator LOT Oriel. The exposure time of the irradiation has been indicated in the figures. Measurements on SAMs on Pt and Au substrates were carried out under nitrogen in order to avoid the substrate oxidation. The bandwidth of the light source in the UV/Vis region was 5 nm. The photoisomerization of the SAMs has been measured as spectral differences to reduce the interference of the metal absorption band. Pt metal surface has been used as a solid substrate in

order to record the spectral differences related to the *trans→cis* isomerization without the contribution of the changes in Surface Plasmon bands of the metal.

b) Kinetic Studies of the trans→cis Isomerization in Solution and on the Surfaces

The maximum *cis* to *trans* ratio in solution of **AZO1** and **AZO2** has been calculated from the ratio of the ^{1}H-NMR signals of the two isomers in the initial and in the photostationary state. The spectrum of the *cis* form has been calculated combining the maximum *cis* to *trans* ratio obtained form the ^{1}H-NMR spectra and the related UV-Vis spectra. The spectra of the measured *trans* and the calculated *cis* form in solution are shown below.

The thermal *cis→trans* back isomerization of **AZO1** and **AZO2**, both in solution and in SAMs, has been followed by recording the increase of UV-Vis spectra at λ = 370 nm and λ = 360 nm, respectively. From these data the lifetimes and the constant rates were calculated. The kinetic constants reported in the main text for the back thermal reaction in solution, on Pt and on Au surfaces are calculated according to a first order kinetic equation.

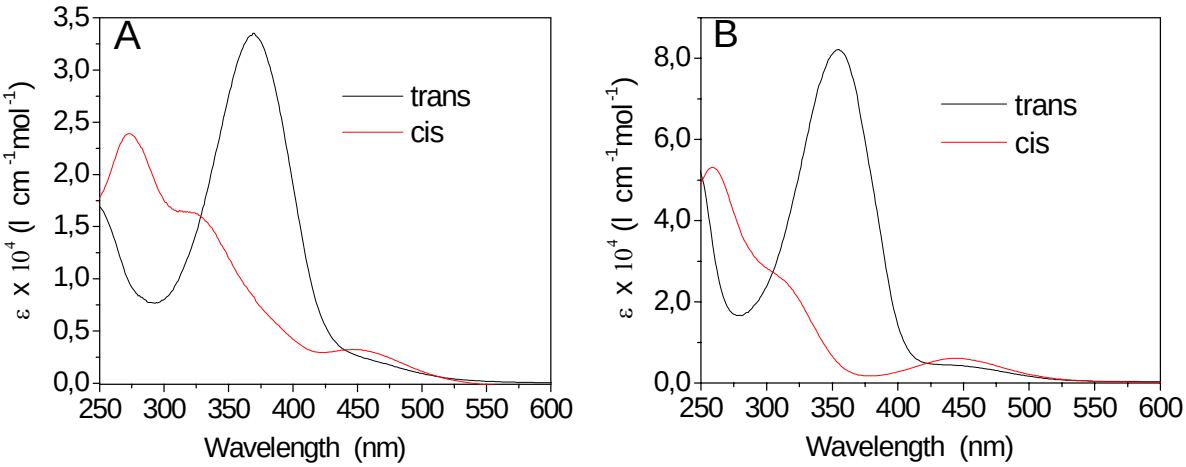

Figure S1: A) Measured UV-Vis absorption spectra of the *trans* form and calculated UV-Vis absorption spectra of the *cis* isomers of **AZO1** and **B) AZO2** in chloroform solution.

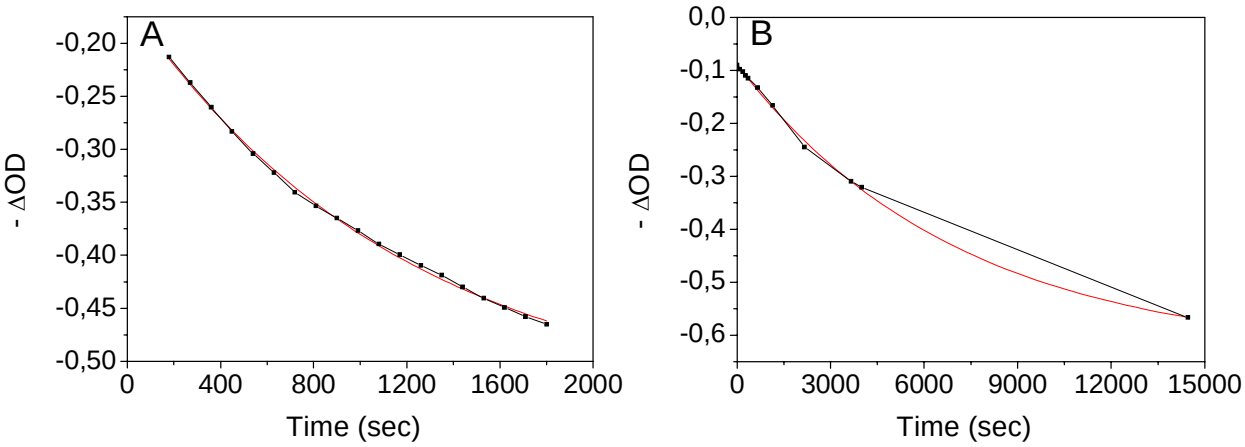

Figure S2: Thermal back reactions in solution: **A**) ΔOD at λ =370 nm for **AZO1** and **B**) ΔOD at λ =360 nm for **AZO2**. The experimental results are displayed in black while the red line displays the fit assuming a first order kinetic.

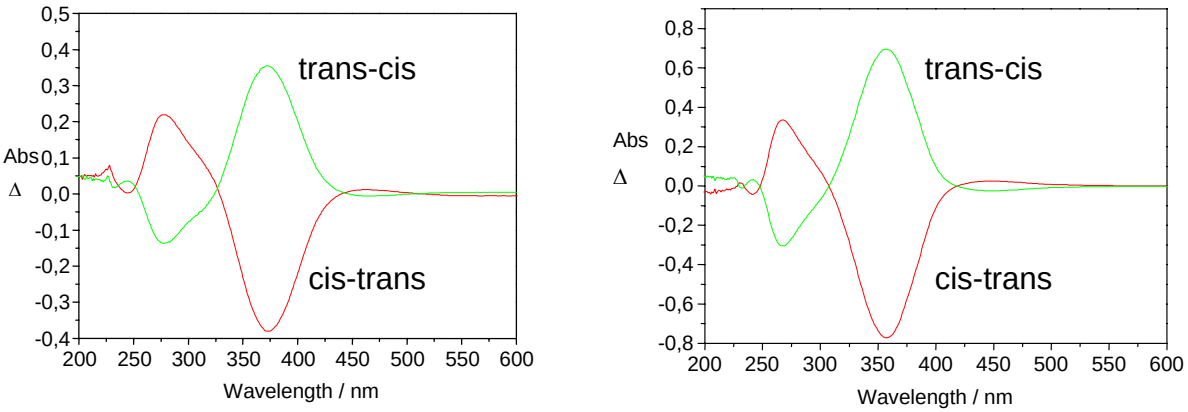

Figure S3: UV-Vis spectral differences obtained in solution for A) **AZO1** under irradiation at λ = 370 nm and B) **AZO2** under irradiation at λ = 360 nm.

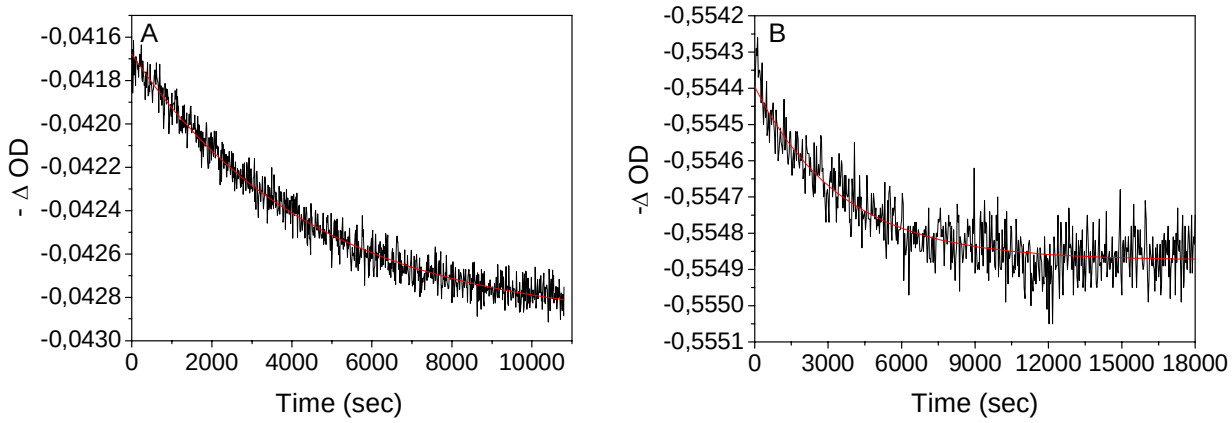

Figure S4: Thermal back reaction of **AZO1** organized in SAMs: ΔOD at λ = 370nm on **A**) Pt and **B**) Au. The experimental results are displayed in black while the red line displays the fit assuming a first order kinetic.

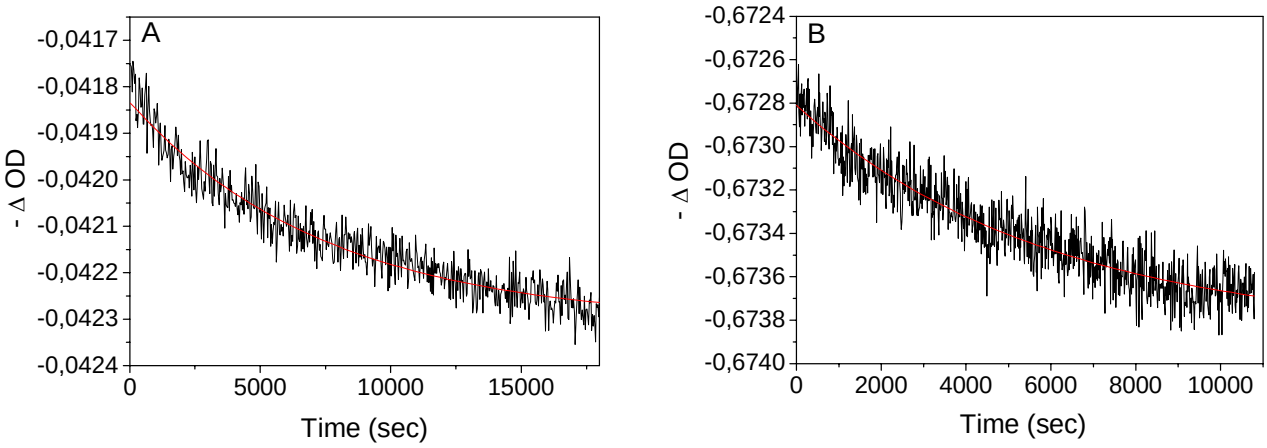

Figure S5: Thermal back reaction of **AZO2** organized in SAMs: ΔOD at λ = 360 nm on **A**) Pt and **B**) Au. The experimental results are displayed in black while the red line displays the fit assuming a first order kinetic.

3. Characterization of Self-Assembled Monolayers (SAMs)

3.1 XPS and NEXAFS Spectroscopy

The SAMs of **AZO1** and **AZO2** were characterized by XPS and NEXAFS spectroscopy. The measurements were performed at room temperature under UHV conditions (base pressure better than 1.5×10^{-9} Torr). The time for the NEXAFS/XPS characterization was selected as a compromise between the spectra quality and the damage induced by X-rays.[4-7]

XPS measurements were performed with two different experimental setups at the HE-TGM 2 beamline of the German synchrotron radiation facility BESSY II in Berlin and at the D1011 beamline of the synchrotron radiation facility Max-lab in Lund, Sweden. The acquisition of the spectra was performed in normal emission geometry using either a VG CLAM 2 (BESSY) or Scienta (MAX-lab) spectrometer. The photon energy was varied from 400 to 660 eV. The energy resolution was either ~0.40 eV (BESSY) or below 0.1 eV (MAX-lab). The binding energy (BE) scale was referenced to the Au $4f_{7/2}$ peak at 84.0 eV.[8] For each sample, a wide scan spectrum and the C 1s, N 1s, S 2p, O 1s and Au 4f or Ag 3d narrow scan spectra were measured. The spectra were normalized to the photon flux and fitted by using a Shirley-type background[9] and symmetric Voigt functions[10] with a Gauss/Lorenz ratio of 4:1. To fit the $Sp_{3/2,1/2}$ doublet, we used a pair of such peaks with the same full width at half-maximum (fwhm), the standard[8] spin-orbit splitting of ~1.2 eV (verified by fit), and the branching ratio of 2 ($Sp_{3/2}/Sp_{1/2}$).

The NEXAFS experiments were performed at the HE-TGM 2 beamline at the German synchrotron radiation facility BESSY II in Berlin. The measurements were carried out at the C and N K-edges in partial electron yield mode with retarding voltages of –150 and –350 V, respectively. Linear polarized synchrotron light with a polarization factor of ~82 % was used. The energy resolution was ~0.40 eV. The incidence angle of the synchrotron light was varied from 90° (**E**-vector in surface plane) to 20° (**E**-vector near surface normal) in steps of 10° - 20° to

monitor the orientational order within the films. This approach is based on so-called linear dichroism in X-ray absorption, that is, the strong dependence of the cross section of the resonant photoexcitation process on the orientation of the electric field vector of the linearly polarized light with respect to the molecular orbital of interest.[11]

The raw NEXAFS spectra were normalized to the incident photon flux by division through a spectrum of a clean, freshly sputtered gold sample. The energy scale was referenced to the pronounced π_1* resonance of highly oriented pyrolitic graphite at 285.35 eV.[12]

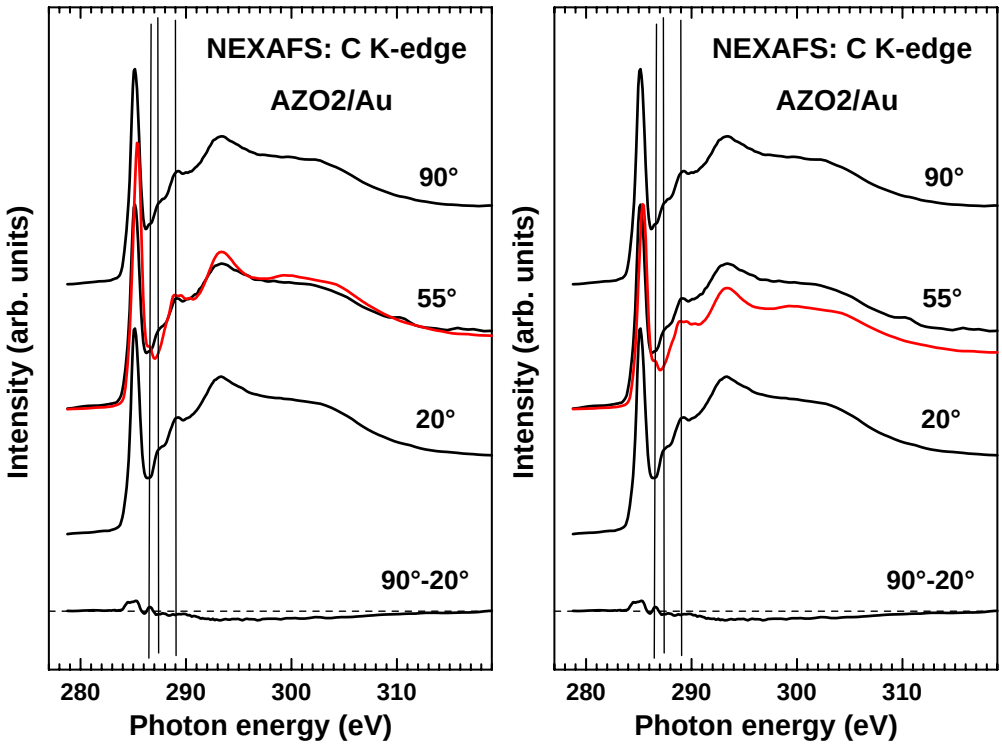

Figure S6: Carbon K-edge NEXAFS spectra of **AZO2**/Au acquired at X-ray incident angles of 90°, 55°, and 20°, respectively, together with the difference between the 90° and 20° spectra. For comparison, the corresponding spectrum of **AZO1**/Au acquired at a X-ray incident angle of 55° is shown in red. The dashed line corresponds to zero.

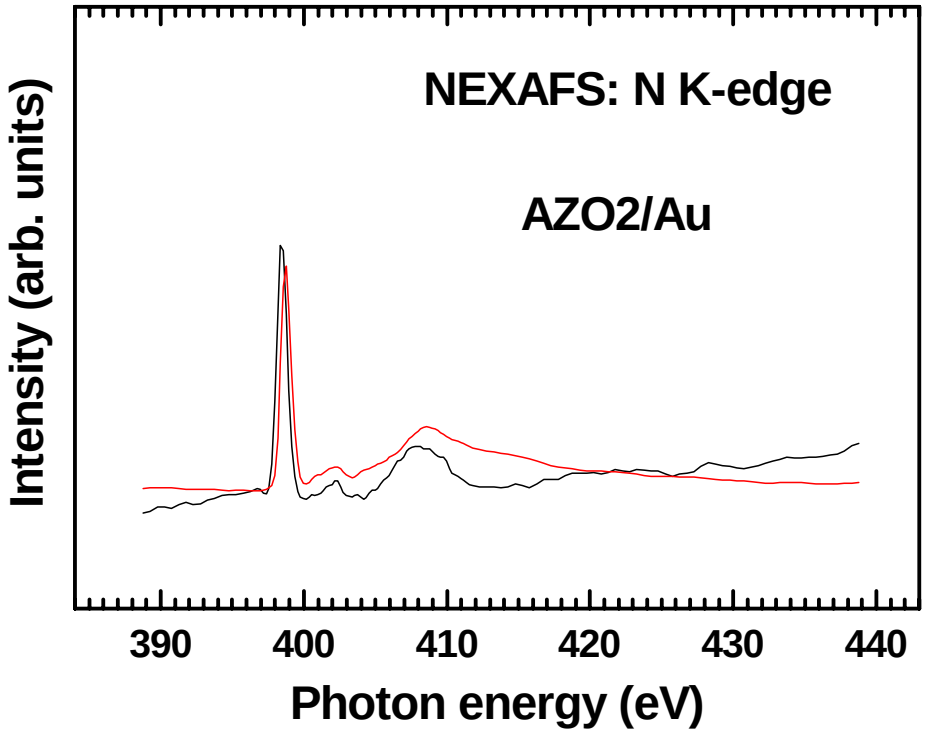

Figure S7: Nitrogen K-edge NEXAFS spectra of **AZO2**/Au acquired at an X-ray incident angle of 55°. For comparison, the corresponding spectrum of **AZO1**/Au acquired at a X-ray incident angle of 55° is shown in red.

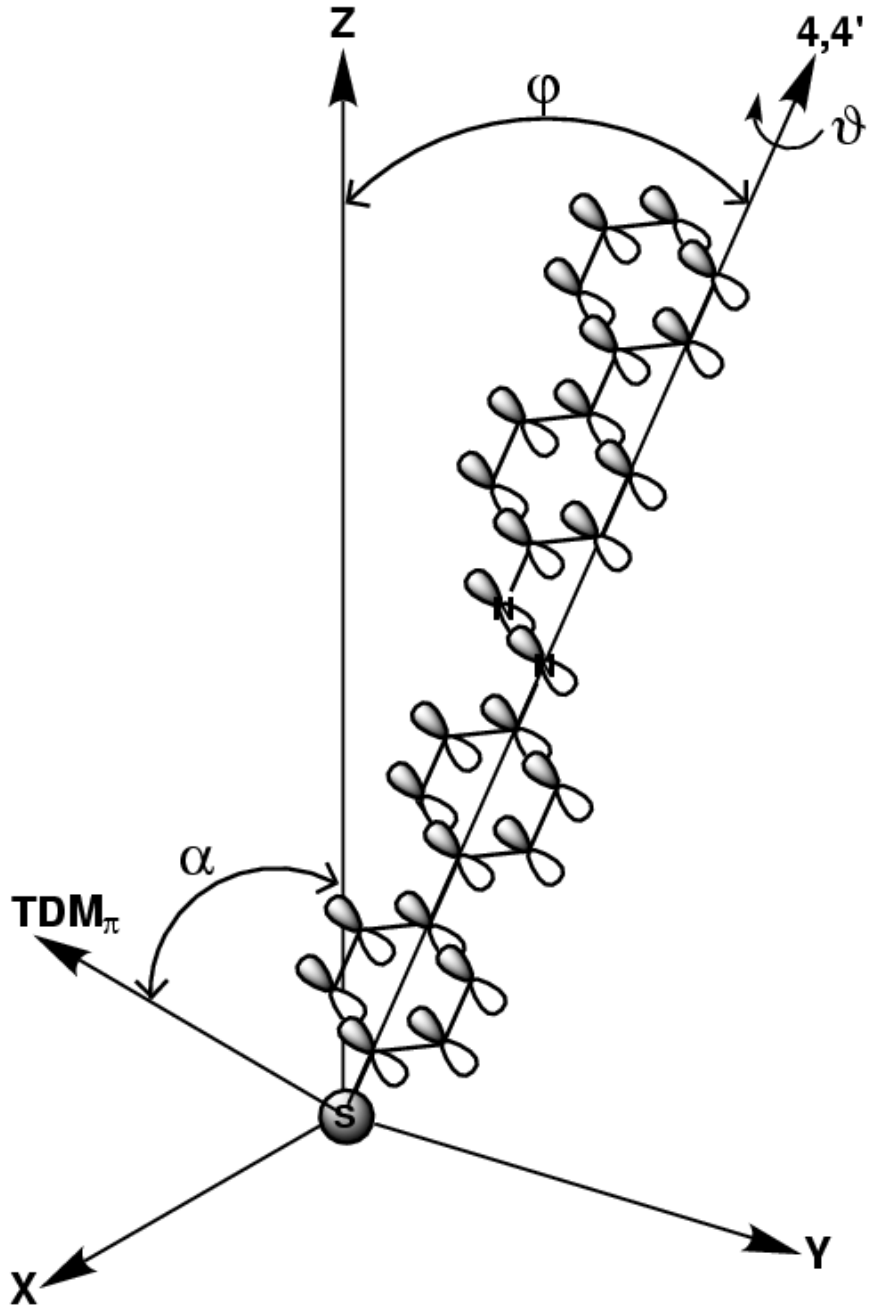

Figure S8: Sketch for the calculation of the tilt angle α used for the characterization of the SAM.

3.1.1 Tilt Angle Calculation

Alongside the qualitative result presented in the main text, the quantitative analysis of the angular dependence of the NEXAFS resonance intensities yields an estimate for the average tilt angle of the **AZO1** molecules in the film.

For this purpose, the intensity of absorption resonances *I* was monitored as a function of the X-ray incidence angle θ and the resulting dependence evaluated according to the theoretical expression for a vector-type orbital[11]

$$I(\alpha,\theta) = A\left\{P \times \tfrac{1}{3}\left[1 + \tfrac{1}{2}\cdot(3\cdot\cos^2\theta - 1)\cdot(3\cdot\cos^2\alpha - 1)\right] + (1-P)\tfrac{1}{2}\sin^2\alpha\right\}, \qquad (1)$$

where *A* is a constant, *P* is a polarization factor of the X-rays, and α is the average tilt angle of the molecular orbital.

For the evaluation, the most pronounced π* resonances at both C and N K-edges were used, representative of the biphenyl and azo moieties, respectively. The respective orbitals are vector ones; they are oriented perpendicular to the ring plane. The transition dipole moment (TDM) of the C1s/N1s → π* transition has then the same orientation, since the C1s and N1s orbitals have a spherical symmetry.

The average tilt angles α of these orbitals have been determined to 73° and 68°, respectively. The accuracy of these values is better than ± 5°.[11] The similarity of these angles suggests that the molecular planes of both biphenyl moieties are almost coplanar and that the π*-orbital of the azo linkage is, as expected, oriented perpendicular to the molecular plane, that is parallel to the π*-orbitals of the phenyl rings. These findings give strong indications that SAMs of **AZO1** are formed by molecules in *trans* conformation.

The π_1* orbital is perpendicular to the plane of the phenyl rings comprising the biphenyl moieties of **AZO1**. Therefore, the derived tilt angle of this orbital is directly related to the tilt angle φ of

the biphenyl axis with respect to the surface normal and to the twist angle ϑ of the aromatic rings with respect to the plane spanned by the surface normal and the biphenyl axis (see Figure S8),[13, 14]

$$\cos \alpha = \cos \vartheta \bullet \sin \varphi \quad (1).$$

Consequently, equation (1) allows the estimation of the tilt angle of the biphenyl axis as soon as some assumptions about the value of the twist angle are made. A high value for the twist angle can be excluded, since it would give rise to a significant molecular tilt, which disagrees with the XPS results presented in the main text. Typically a twist angle ϑ of 32° is observed for bulk aromatic compounds exhibiting, as a rule, a herringbone molecular packing.[15-18] Similar structures[1, 19] and a planar conformation of oligophenyl moieties are also expected to occur in SAMs of aromatic constituents.[1, 19, 20] Hence, for our system the most reasonable supposition for the twist angle is 32°. Assuming this angle ϑ for the biphenyl moieties comprising the **AZO1** molecule, we obtained an average molecular tilt angle φ of 20.5°.

3.2 Cyclic Voltammetry (CV) Measurements

Cyclic Voltammetry (CV) measurements were obtained with an Autolab PGSTAT100 apparatus at room temperature. A standard three-electrode configuration was used with a SAM-coated gold electrode as the working electrode, Ag/AgCl as the reference electrode, and a platinum wire as the counter electrode in a glass vessel.

The SAMs were prepared by immersion of the working gold electrode (2 mm in diameter) into a $5*10^{-4}$ M chloroform solution of **AZO1** and **AZO2**, respectively, and in $1*10^{-3}$ M ethanol solution of $C_{11}H_{24}S$. After 18 hours of immersion under nitrogen atmosphere, the electrode was carefully rinsed with chloroform or ethanol, blow dried under nitrogen and immediately put in the CV set-up for the measurements.

The solution used in the electrochemical cell for performing the blocking experiment contained $1*10^{-3}$ M of the redox agent $K_3[Fe(CN)_6]$ dissolved in 1 M KCl/water solution. The sweep rate was set at 50 mV s^{-1} for this measurement.

The reductive desorption cyclic voltammograms were recorded in 0.5 M KOH/water solution at 100mV/s. The current was taken to be negative when the reductive desorption proceeded.

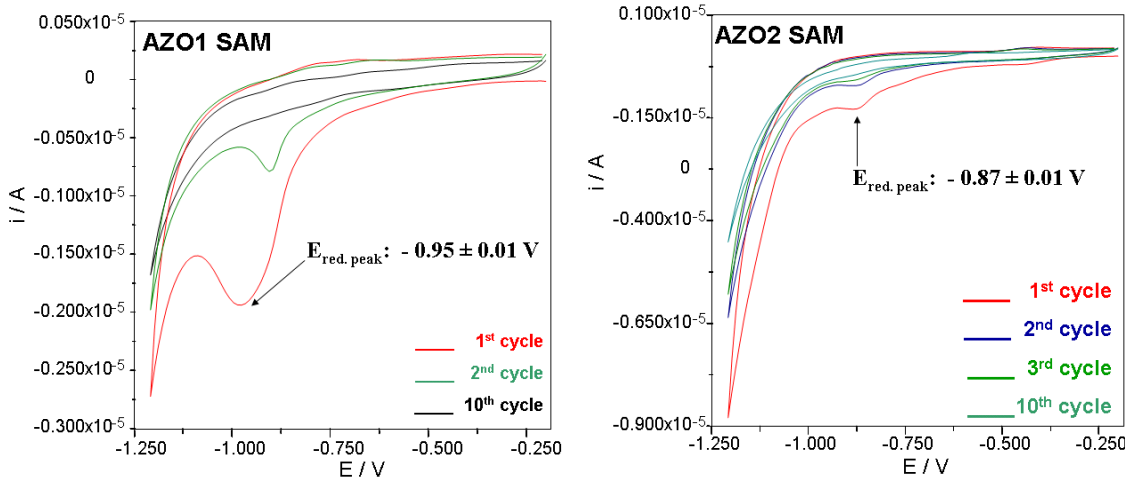

Figure S9: Subsequent CV scans on gold electrode coated with a SAM of **AZO1** and **AZO2** (0.5 M KOH, 100 mV/s).

3.3 Scanning Tunneling Microscopy (STM) Measurements

STM images were obtained in constant current mode with a commercial apparatus (multimode Nanoscope IV, Veeco) in air and at room temperature. The STM tips were cut or chemically etched from a Pt/Ir wire (0.25 mm). Unit cells were averaged over several images making use of SPIP software (Scanning Probe Image Processor (SPIP) version 2.0 image metrology ApS, Lyngby, Denmark).

Mica was freshly cleaved and baked at 450° for 5 h in a high vacuum chamber (10^{-7} mbar). Subsequently, 100-150 nm of gold were evaporated onto the mica substrate. The substrates were kept under a dry atmosphere until their use for the SAM chemisorption. Before immersion in the solutions of **AZO1** or **AZO2** the gold substrates were annealed with a butane flame. This procedure leads to atomically flat surfaces that typically extend over several hundred nanometers. The trans SAMs of both azo-compounds were formed after overnight incubation in the dark of the Au(111) in a $5*10^{-4}$ M solution of **AZO1** and **AZO2** in toluene or $CHCl_3$. STM imaging experiments showed the same molecular packing formed by **AZO1** on gold substrate for concentrations ranging from 10^{-4} M to 10^{-3} M in chloroform as well as toluene.

3.3.1 Scan Angle Effect on STM Image Contrast

In previous STM studies of azobenzene-substituted alkylthiolate SAMs on Au(111) two types of domains with different STM contrasts have been found, viz. an herringbone and a pseudo-hexagonal lattice.[21] While both domains possess identical unit cell parameters and contain two molecules, the second molecule was found to locate either at the center of the unit cell or displaced towards one of its corners giving rise to either a pseudo-hexagonal lattice or an herringbone lattice, respectively.

We also observed two different types of domains in **AZO1** SAMs. But the observed lattice structure seems to depend on the angle used to record the image. The herringbone and pseudo-hexagonal cell has been observed for domain B and A recorded at 90°, -15° and 0°, respectively (Figure S10 and S11). For **AZO1** SAMs we observed two types of domains, e.g. domains marked with A in Figure S10A show a herringbone structure with the same unit cell and image contrast as the trans-domains in Figure 9 (main text). Significantly, upon rotation of the scan angle used during the image acquisition ($\Delta\theta_{b\text{-}a}$= 90°) identical domains display a pseudo-hexagonal lattice, e. g. domain A in Figure S10A and after rotation in Figure S10C. After further rotation of the scan angle to $\Delta\theta_{b\text{-}d}$= +15° the domain B in Figure S10B exhibits again a different contrast than in Figure S10D.

Similar behavior has been found simultaneously for domains B and A, which feature different orientations. Therefore, imaging artifacts can be ruled out. STM-tip induced processes can be excluded, because the same contrast variation has been found using asymmetric (prepared by mechanical cut) and symmetric STM tips (fabricated by chemical etching). Furthermore, the contrast variation was found to be completely reversible upon reverse scan angle rotation.[21] Hence, the presence of two non-equivalent Au-S binding sites can be neglected. Due to the high rigidity of **AZO1** the scan angle effect is most likely not caused by different chain conformations,

as described for SAMs of comparably flexible alkanethiols.[22] Furthermore, the effect cannot be explained by a change in binding sites, because similar results have already been reported using Atomic Force Microscopy (AFM) on SAMs of alkylthiols with azobenzene headgroups.[23] In the last measurements changes in the image contrast can only be attributed to the orientation of the upper phenyl ring of the azo-headgroup. According to Heckl and co-workers[24] who observed a similar scan angle effect in STM imaging of molecular adsorbates, such an effect is caused by the dependence of the polarizability of the molecular bonds on the scan angle, which is induced by the electric field of the tip.

In view of the above arguments, we suggest that the observed scan angle effect can be attributed to the influence of the symmetry of the molecular orbitals contributing to the tunneling because, given the herringbone arrangement, the orientation of the molecular orbitals of the two **AZO1** molecules in the unit cell differs with respect to the scan direction of the tip. This probable contribution of the molecular orbitals to the tunneling indicates that the described scan angle effect is not merely caused by the density of electronic states localized at the Au-S bond.[25]

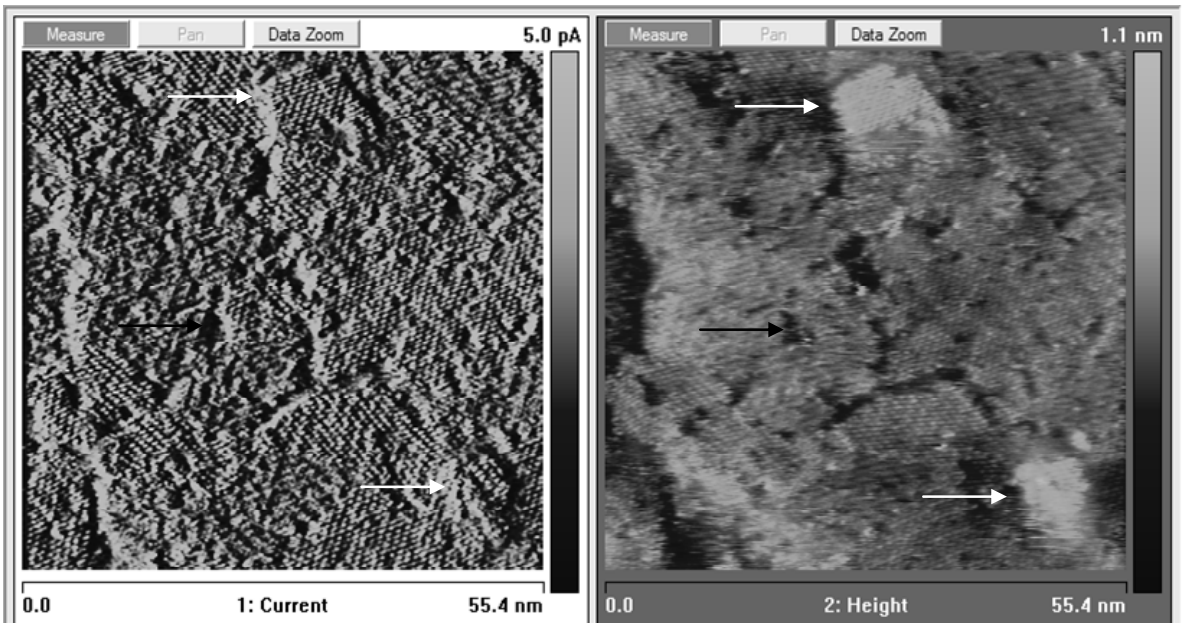

Figure S10: STM image showing high-resolution current (left) and height (right) images of the **AZO1** monolayer on Au(111). Adatoms are indicated by white arrows and the etched pits by the black arrows. The highlands of adatoms are formed from surface gold atoms that diffuse and reorganize on top of the gold substrate, as a consequence of a surface gold lattice relaxation occurring in response to the stress induced by the SAM binding. Their height has been measured to be 2.4 Ǻngstroms as typically observed for monoatomic gold steps.

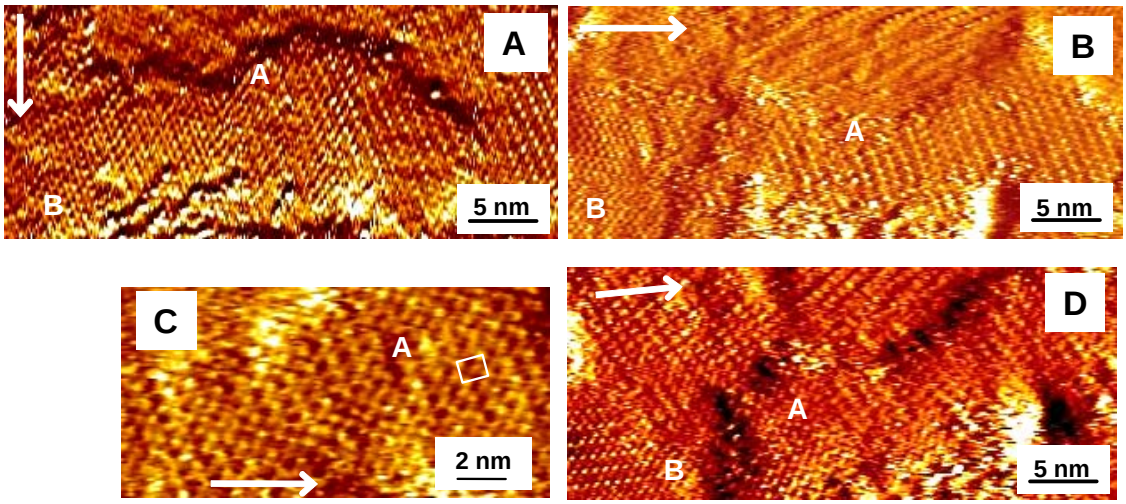

Figure S11. Constant-current images of SAM of **AZO1**. White arrows indicate the image scan direction. **A)** Image of the initial scan; **B)** Image obtained on the same area as for image A, but after scan angle rotation of 90° (clockwise rotation); **C)** Zoom on image B; **D)** Image obtained on the same area as for B), but after scan angle rotation of 15° (anticlockwise rotation). I_T = 15.0 pA and V_T = 245 mV.

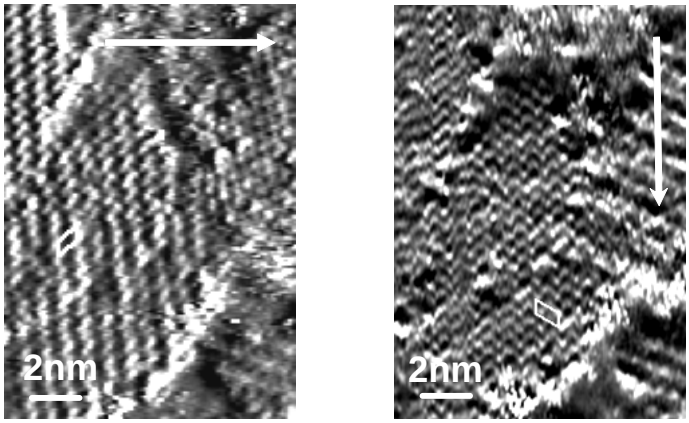

Figure S12: STM images showing current images of the **AZO1** monolayer on Au(111). Left: unit cell parameters: a= (0.60 ± 0.05) nm; b= (1.0 ± 0.05) nm: Right: same area after 90° rotation of the scan angle: a= (0.60 ± 0.05) nm; b= (1.1 ± 0.05) nm. Arrows indicate the scan direction.

4. References

[1] A. Shaporenko, M. Elbing, A. Błaszczyk, C. v. Hänisch, M. Mayor, M. Zharnikov, *J. Phys. Chem. B* **2006**, *110*, 4307-4317.

[2] T. Haack, L. Erdinger, G. Boche, *Mutat. Res.* **2001**, *491*, 183-194.

[3] M. Janczewski, W. Charmas, *Chem. Abstr.* **1967**, *66*, 37570z.

[4] M. Wirde, U. Gelius, T. Dunbar, D. L. Allara, *Nucl. Instrum. Methods Phys. Res., Sect. B* **1997**, *131*.

[5] B. Jäger, H. Schürmann, H. U. Müller, H.-J. Himmel, M. Neumann, M. Grunze, C. Wöll, *Z. Phys. Chem.* **1997**, *202*, 263-272.

[6] K. Heister, M. Zharnikov, M. Grunze, L. S. O. Johansson, A. Ulman, *Langmuir* **2001**, *17*, 8-11.

[7] M. Zharnikov, M. Grunze, *J. Vac. Sci. Technol. B* **2002**, *20*, 1793-1807.

[8] J. F. Moulder, W. E. Stickle, P. E. Sobol, K. D. Bomben, in *Handbook of X-ray Photoelectron Spectroscopy* (Ed.: J. Chastian), Perkin-Elmer Corp., Eden Prairie, MN, **1979**.

[9] D. A. Shirley, *Phys. Rev. B* **1972**, *5*, 4709-4714.

[10] G. K. Wertheim, M. A. Butler, K. W. West, D. N. E. Buchanan, *Rev. Sci. Instrum.* **1974**, *45*, 1369-1371.

[11] J. Stöhr, *NEXAFS Spectroscopy*, Springer-Verlag, Berlin, **1992**.

[12] P. E. Batson, *Phys. Rev. B* **1993**, *48*, 2608-2610.

[13] M. Zharnikov, A. Küller, A. Shaporenko, E. Schmidt, W. Eck, *Langmuir* **2003**, *19*, 4682-4687.

[14] A. Shaporenko, K. Adlkofer, L. S. O. Johansson, M. Tanaka, M. Zharnikov, *Langmuir* **2003**, *19*, 4992-4998.

[15] D. W. J. Cruickshank, *Acta Cryst.* **1956**, *9*, 915-923.

[16] J. Trotter, *Acta Cryst.* **1961**, *14*, 1135-1140.

[17] I. A. Kitaigorodskii, *Organic Chemical Crystallography*, Consultants Bureau, New York, **1961**.

[18] G.-P. Charbonneau, Y. Delugeard, *Acta Cryst.* **1976**, *B32*, 1420-1423.

[19] H.-J. Himmel, A. Terfort, C. Wöll, *J. Am. Chem. Soc.* **1998**, *120*, 12069-12074.

[20] J. F. Kang, A. Ulman, S. Liao, R. Jordan, G. Yang, G.-y. Liu, *Langmuir* **2001**, *17*, 95-106.

[21] S. C. B. Mannsfeld, T. W. Canzler, T. Fritz, H. Proehl, K. Leo, S. Stumpf, G. Goretzki, K. Gloe, *J. Phys. Chem. B* **2002**, *106*, 2255-2260.

[22] G. E. Poirier, *Chem. Rev.* **1997**, *97*, 1117-1128.

[23] M. Jaschke, H. Schönherr, H. Wolf, H.-J. Butt, E. Bamberg, M. K. Besocke, H. Ringsdorf, *J. Phys. Chem.* **1996**, *100*, 2290-2301.

[24] S. J. Sowerby, M. Edelwirth, M. Reiter, W. M. Heckl, *Langmuir* **1998**, *14*, 5195-5202.

[25] R. R. Nazmutdinov, J. Zhang, T. T. Zinkicheva, I. R. Manyurov, J. Ulstrup, *Langmuir* **2006**, *22*, 7556-7567.